REPORT

PROTEIN FOLDING

Hidden dynamics in the unfolding of individual bacteriorhodopsin proteins

Hao Yu,[1]* Matthew G. W. Siewny,[1,2]* Devin T. Edwards,[1]
Aric W. Sanders,[3] Thomas T. Perkins[1,4]†

Protein folding occurs as a set of transitions between structural states within an energy landscape. An oversimplified view of the folding process emerges when transiently populated states are undetected because of limited instrumental resolution. Using force spectroscopy optimized for 1-microsecond resolution, we reexamined the unfolding of individual bacteriorhodopsin molecules in native lipid bilayers. The experimental data reveal the unfolding pathway in unprecedented detail. Numerous newly detected intermediates—many separated by as few as two or three amino acids—exhibited complex dynamics, including frequent refolding and state occupancies of <10 μs. Equilibrium measurements between such states enabled the folding free-energy landscape to be deduced. These results sharpen the picture of the mechanical unfolding of membrane proteins and, more broadly, enable experimental access to previously obscured protein dynamics.

Elucidating the process by which a protein folds into its native structure is a large, interdisciplinary field (*1*). Proper identification of the intermediate states along the protein-folding pathway is essential to describe the folding process accurately. Advances in ensemble techniques have led to the characterization of previously "invisible" folding intermediates (*2*). Single-molecule techniques, including fluorescence (*3*, *4*) and force spectroscopy (*5*–*7*), have proven especially valuable for detecting sparsely populated intermediates. In particular, force spectroscopy studies have yielded kinetic insights into the unfolding pathways of diverse macromolecules, including globular proteins (*8*), membrane proteins (*9*), multiprotein complexes (*10*), and ribozymes (*11*). These studies have identified the energy barriers between states and distinguished among obligatory, nonobligatory, and off-pathway intermediates. However, critical kinetic information is obscured whenever closely spaced and/or transiently occupied intermediates remain undetected (Fig. 1A). For example, limited experimental precision can lead to two closely spaced states being misinterpreted as a single composite state exhibiting nonexponential lifetimes (*8*). Moreover, limited temporal resolution can lead to artifacts in force spectroscopy studies (*12*, *13*), and theoretical simulations suggest that state occupancies that are brief relative to the response time of the force probe remain undetected (*12*). Beyond such identified limitations, it remains challenging to characterize conformational dynamics on the microsecond-to-millisecond time scale in many single-molecule assays, particularly for subtle changes in structure.

Advanced, single-molecule force spectroscopy (SMFS) assays typically have a temporal resolution of ~50 to 100 μs (*14*), with recent optical-trapping work opening the door to probing dynamics with ~6- to 10-μs resolution (*15*). On still faster time scales, atomic force microscopy (AFM) by using ultrashort cantilevers [length (L) = 9 μm] has unfolded a globular protein at high speed (4 mm/s) with 0.5-μs time resolution (*16*). We unfolded bacteriorhodopsin (BR), a model membrane protein, with ultrashort cantilevers optimized for 1-μs SMFS (fig. S1) (*17*) and thereby uncovered previously unobserved protein dynamics and intermediates. We elucidated the unfolding pathway with improved precision and resolved a long-standing discrepancy in the size scale of the fundamental structural elements involved in BR unfolding, as deduced from experiments (*18*–*22*) or molecular dynamics (MD) (*23*).

SMFS studies of BR represent an important model system with which to test the experimental boundaries of protein unfolding. Prior work has shown that the BR-unfolding pathway (*18*) has a comparable number of structural intermediates with that of the fourfold larger molecule Hsp90 (*24*). Although mechanical unfolding is not the simple reversal of translocon-mediated membrane protein folding, AFM-based BR studies provide a window into quantifying the energetics of individual membrane proteins embedded in a native lipid bilayer (purple membrane for BR) (*9*) and the size scale of detectable structural intermediates (*18*, *19*). Such studies have been extended to diverse classes of membrane proteins (*19*), including biomedically important G protein–coupled receptors (GPCRs) to which BR is homologous.

A consensus unfolding pathway for BR emerged early on (*18*), and this pathway has been validated over the past 15 years with the number and location of BR's unfolding intermediates remaining essentially unchanged across different supporting substrates (mica, glass, and purple membrane) (*19*). The assay is initiated by pressing an AFM tip into the membrane to promote a nonspecific attachment of the tip to the cytoplasmic end of the G-helix of BR (Fig. 1B). The cantilever is then retracted at a fixed velocity (v) while measuring force via cantilever deflection.

When using our optimized ultrashort cantilevers to extend BR at 300 nm/s, force-extension curves displayed three major intermediates (Fig. 1C), recapitulating previous studies (*9*, *19*). The elasticity of the unfolded segment of the protein associated with each of these states was well described by a worm-like-chain (WLC) model (Fig. 1C, colored curves). Each major intermediate occurred after fully unfolding the previous pair of helices and was previously determined to be obligate intermediates (*18*–*22*). In other words, the unfolding pathway is dominated by the topology of the protein in the lipid bilayer. Nonobligate minor intermediates (states not fitted with the WLC model in Fig. 1C) occurred after each major state, although with lower probability of occupancy (table S1). The GF helix pair unfolds at very low extension and is generally excluded from analysis because of confounding signals associated with variability in adhesion between the tip and surface (*19*).

Closer inspection of our resulting force-extension curves uncovered a strikingly complex, dynamic folding network (Fig. 1, D to F). The optimized ultrashort AFM cantilever gave a ~100-fold improvement in temporal resolution and a ~10-fold improvement in force precision (fig. S1). In particular, the data showed a large increase in the number of states that could be resolved while unfolding the ED, CB, and A helices (Fig. 1, D to F, respectively). For example, whereas prior studies over the past 15 years reported two nonobligate intermediates when unfolding the ED helix pair (Fig. 1D, top left inset) (*18*–*22*), we observed 14 intermediates (Fig. 1D and fig. S2), denoted I_{ED}^{1} to I_{ED}^{14}. Newly identified intermediates were detected throughout the unfolding pathway. For the CB helix pair (Fig. 1E) and helix A (Fig. 1F), we observed a threefold or larger increase in the number of resolved intermediates as compared with the consensus number of observed intermediates (*18*–*22*). Changes in secondary structure associated with each intermediate were assigned according to changes in contour length (ΔL_0) derived from WLC fits to the data, with an estimated uncertainty along the polypeptide of ±1 amino acid (table S1).

Most of the intermediates were closely spaced and transiently populated, making them difficult to detect. On the basis of the extension changes, we resolved transitions corresponding to the unwinding of just two amino acids (for example,

[1]JILA, National Institute of Standards and Technology and University of Colorado, Boulder, CO 80309, USA. [2]Department of Physics, University of Colorado, Boulder, CO 80309, USA. [3]Radio Frequency Technology Division, National Institute of Standard and Technology, Boulder, CO 80305, USA. [4]Department of Molecular, Cellular, and Developmental Biology, University of Colorado, Boulder, CO 80309, USA.
*These authors contributed equally to this work. †Corresponding author. Email: tperkins@jila.colorado.edu

$I^{4}_{ED}\leftrightarrow I^{5}_{ED}$; $I^{9}_{ED}\leftrightarrow I^{10}_{ED}$; and $I^{11}_{ED}\leftrightarrow I^{12}_{ED}$) (Fig. 2 and fig. S2) or half an α-helical turn. Moreover, dwell times as short as 8 μs could be resolved (Fig. 2B). Such fleeting times are commonly associated with transition path times between states (*15*, *25*), rather than state occupancy times resolved in a single record. In addition, as a result of increased precision, one previously identified major obligate intermediate (I^{0}_{CB}), which occurs after fully unfolding the ED helix pair, is actually composed of two nonobligatory states separated by five amino acids. The proportion of trajectories that goes directly into I^{1}_{CB} without a detectable occupancy in I^{0}_{CB} increases as pulling velocity is increased from v = 30 to 3000 nm/s (fig. S3). Last, a small percentage (13%) of molecules exhibited at least one continuous, rather than discrete, transition (fig. S4). Additional data and more advanced modeling will be required to unravel the mechanism(s) underlying such continuous transitions.

Refolding of individual BR molecules has been observed as the AFM tip is brought closer to the surface (v < 0 nm/s) (*26*), which lowers the force on the unfolded molecule and promotes folding. In contrast, BR refolding has not been detected while retracting the cantilever (v > 0 nm/s), implying that the standard rapid stretching assay was far from equilibrium. With our improved spatiotemporal resolution, we now routinely detect reversible transitions between two (Fig. 1, D to F, bottom inset; and fig. S5) and even three states (Fig. 2) while stretching. Rapid, back-and-forth transitions have been called a hallmark of equilibrium between states (*27*), but technically, these states are only near equilibrium because the

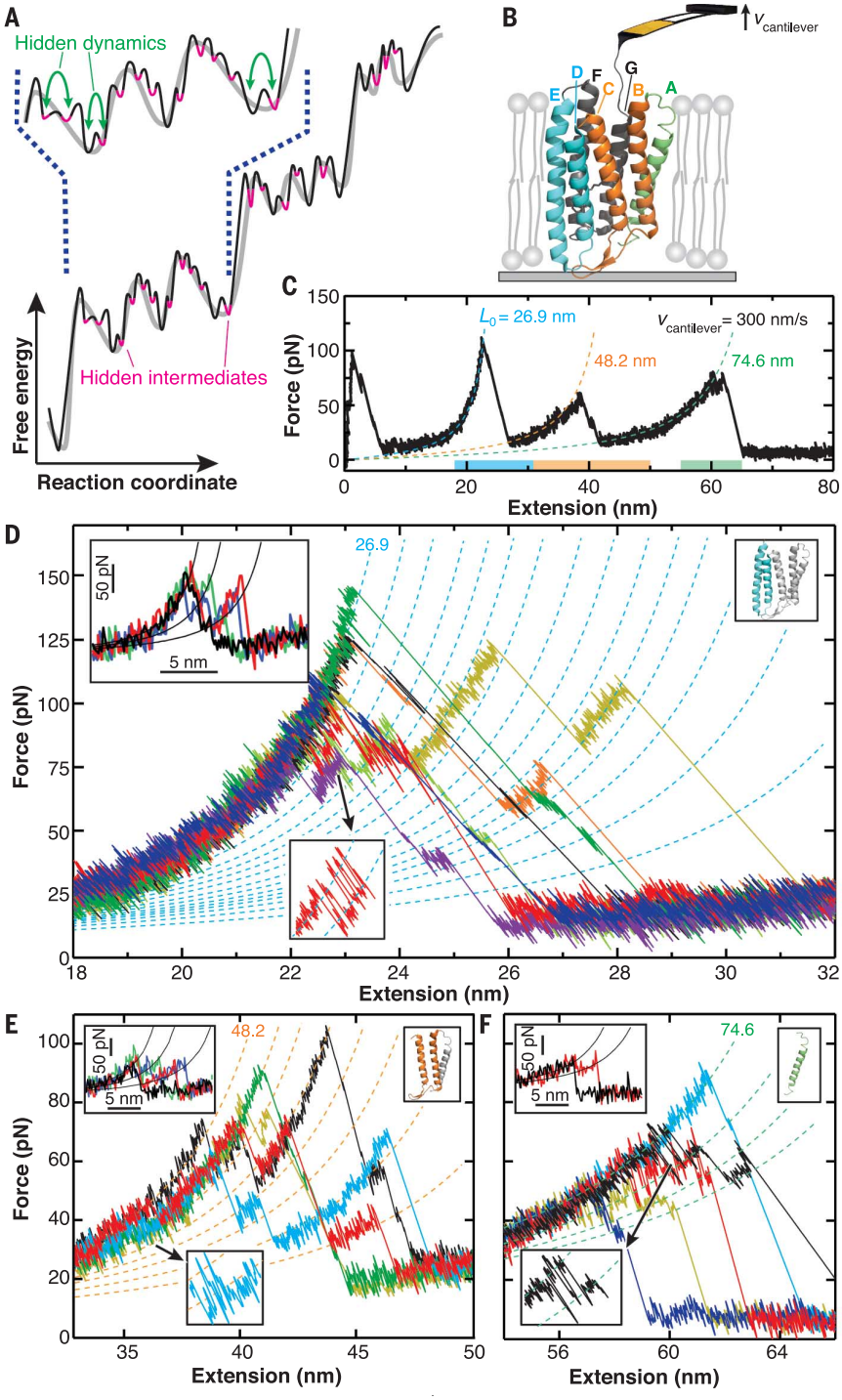

Fig. 1. SMFS of BR measured with 1-μs temporal resolution. (**A**) A conceptual sketch shows a low- (gray) and a high-resolution (black) representation of the same free-energy landscape. Each free-energy valley represents an intermediate, with lower energy and therefore more fully folded states depicted on the left whereas higher-energy, more unfolded states are shown on the right. Assays with improved sensitivity enable the detection of previously hidden folding intermediates (magenta) and protein dynamics between closely spaced states separated by low barriers (green arrows). (**B**) An illustration of the unfolding of individual BR molecules by a modified ultrashort cantilever. Mechanical unfolding occurs by retracting the cantilever at a constant velocity. Each transmembrane helix is identified by its standard letter label. (**C**) A typical force-extension curve (FEC) acquired by using a modified ultrashort cantilever recapitulates the three previously detected major intermediates corresponding to pulling on the top of E (light blue), C (orange), and A (green) helices. The FEC segments associated with these major states are well described by a worm-like chain model (colored dashed lines) and labeled with their associated contour lengths. The colored bars denote the extension range in (D) to (F). (**D**) Representative high-resolution FECs reveal 14 intermediates when unfolding the ED helix pair. In contrast, two intermediates were reported in prior studies (top left inset) (*18*–*22*). [This inset and the corresponding insets in (E) and (F) are reprinted from (*20*) with permission from Elsevier.] (**E**) FECs show seven intermediates during the unfolding of the CB helix pair instead of two observed previously (*18*–*22*). (**F**) FECs show three intermediates while unfolding helix A instead of one observed previously (*18*–*22*). Near-equilibrium fluctuations between multiple states were observed when stretching at 300 nm/s [(D) to (F), bottom inset; force-time curves are available in fig. S5].

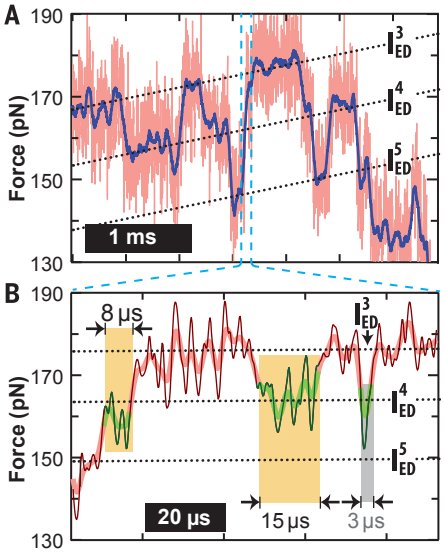

Fig. 2. Improved spatiotemporal resolution details complex and rapid dynamics between closely spaced states. (**A**) Force-versus-time trace shows rapid back-and-forth transitions between three states determined with hidden-Markov-model analysis (black dotted lines) and correspond to I^3_{ED}, I^4_{ED}, and I^5_{ED}. Data were smoothed to 10 kHz (blue) and 200 kHz (pink), respectively. A highlighted portion of the trace (light blue) is shown in detail in (B). (**B**) High-resolution force-versus-time trace illustrates rapid dynamics between I^3_{ED}, I^4_{ED} (green), and I^5_{ED}. Here, two state lifetimes of 15 and 8 µs are identified with a hidden-Markov-model analysis (orange). A potentially even shorter state lifetime of 3 µs (gray) is seen but not identified as a state by the hidden-Markov-model analysis. Traces were smoothed to 100 kHz (light colors) and 830 kHz (dark colors).

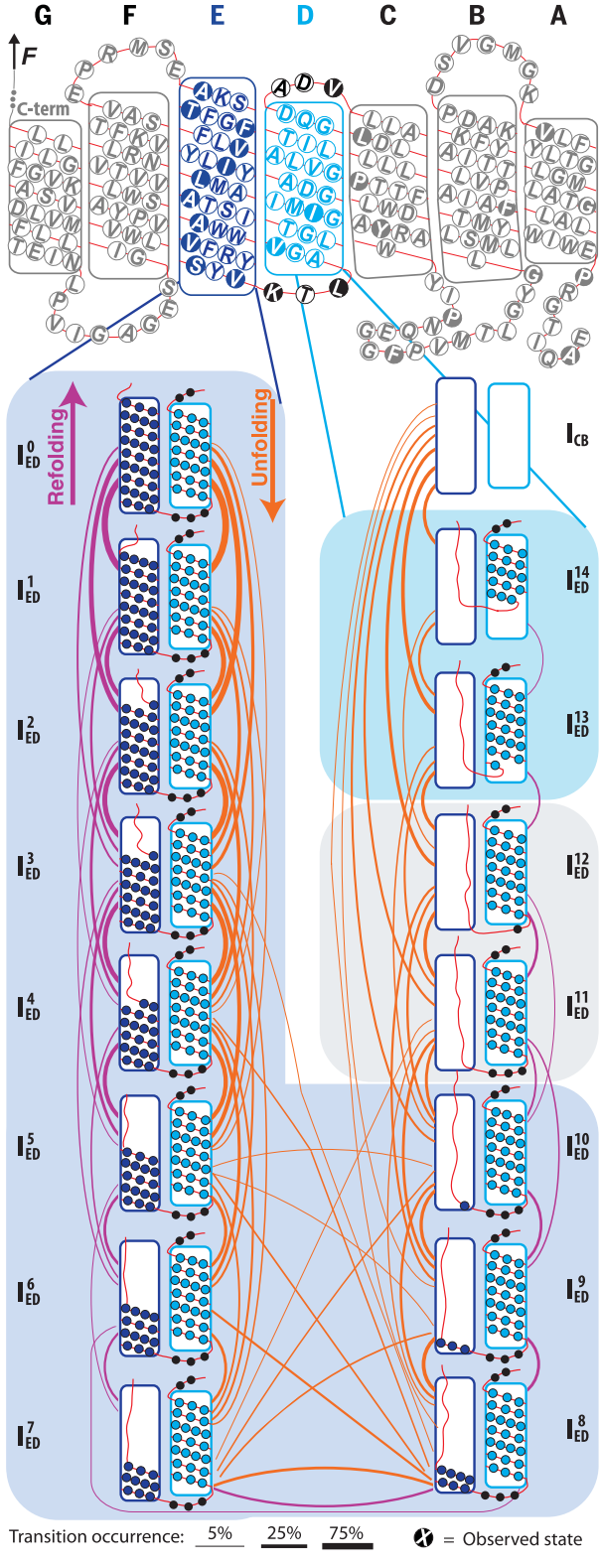

Fig. 3. Unfolding pathway for the ED helix pair. (**Top**) Illustration of the primary and secondary structure of BR. Locations of observed folding intermediates are indicated by residues with solid circles. (**Bottom**) Each helix pair diagram depicts an observed intermediate state, with connecting lines representing transitions observed in at least four (of 98) different molecules containing a total of 1399 transitions. Orange lines represent unfolding transitions, and purple lines show refolding transitions. Line widths represent the frequency of observing a particular transition. The analogous unfolding pathways for the CB helix pair and the A helix are shown in fig. S7, and an alternative matrix representation is shown in fig. S8.

force acting on each state varies slightly in time. Unexpectedly, these near-equilibrium transitions occurred even at a high stretching rate (v = 300 nm/s) compared with prior reports of similar dynamics in globular proteins (v = 1 to 10 nm/s) (*27*, *28*). Indeed, back-and-forth transitions in BR persisted up to the highest velocities examined (5000 nm/s) (fig. S6) and were observed in all three major regions (ED, CB, and A). These states exhibited brief lifetimes (<1 ms) and could refold against comparatively high loads [force (F) ≈ 30 to 160 pN]. Refolding was most frequently observed between states located near the top of helix E and helix A (70% of molecules refolded from I^1_{ED} to I^0_{ED}; 90% of molecules refolded from I^1_A to I^0_A). Moreover, refolding at v = 300 nm/s was ubiquitous; all records exhibited at least one refolding event in the ED helix pair.

Widespread refolding, together with the large number of resolved intermediates, led to highly varied trajectories along a multistate unfolding pathway (Fig. 1, D to F). Displayed in Fig. 3 is the unfolding (Fig. 3, orange lines) and refolding (Fig. 3, purple line) transitions observed during the unfolding of the ED helix pair. The sheer complexity of the data set obtained here prevents broad generalizations, but the density of the intermediate states, 80% separated by just two or three amino acids, indicates that the structural elements associated with BR unfolding are much smaller than previously experimentally reported; prior reports have described the unfolding process as occurring in units of pairs of helices, a single helix, or approximately half a helix (*19*). Thus, the improved spatiotemporal resolution used here has uncovered an underlying

free-energy landscape that is much more complex than any such landscape previously described by other experimental methods to date (*29*). Fully characterizing this free-energy landscape of a multistate system from dynamic experiments ($v \neq 0$ nm/s) requires a theoretical framework that can account for nonequilibrium interconversions among multiple states (Fig. 2), such as the formalism developed by Zhang and Dudko (*30*). However, given the multiplicity of unfolding trajectories through the unfolding pathway (Fig. 3 and figs. S7 and S8), the numerous intermediate states (>25), the brief state lifetimes (<1 ms), and the presence of refolding, a substantially larger data set is needed to apply such an analysis. Hence, the current work points to a need for further technical advances that would yield a 10- to 100-fold increase in the number of records at 1-μs or better resolution.

True equilibrium folding between select rapidly interconverting states, a new regime for membrane proteins, was achieved. Specifically, the force in each state was constant in time, similar to optical-trapping studies of globular proteins (*8*, *29*). In our AFM-based assay, we retracted the tip in a series of steps in the vicinity of I^1_{ED} and I^2_{ED} and thereby measured ~100 transitions at each stationary condition (v = 0 nm/s) (Fig. 4A and fig. S9). As expected, the equilibrium shifted from I^1_{ED} to I^2_{ED} as the tip-sample separation (and therefore the force) in each state increased. These states were closely spaced (three amino acids) and transiently populated, with dwell times of 15 μs well-resolved (Fig. 4B).

A powerful aspect of SMFS is that a one-dimensional (1D) free-energy landscape can be reconstructed from equilibrium trajectories as a function of load, with the molecular extension serving as the reaction coordinate. A variety of theoretical methods have been developed to derive such landscapes from data (*29*). Here, we used p_{fold} analysis (*31*) because it is less sensitive to instrumental compliance issues, as shown recently by using well-characterized DNA hairpins (*32*). In this work, we applied p_{fold} to equilibrium BR records between I^1_{ED} and I^2_{ED} (Fig. 4A) to calculate the free-energy landscape at $F_{1/2}$, the force at which both states are equally occupied (Fig. 4C and fig. S10). Extrapolating the energy difference between states to zero applied force (ΔG_0) yielded ΔG_0 = 8.0 ± 0.4 kcal/mol. Because this transition involves unfolding three amino acids (T-F-G) of the transmembrane helix, the average ΔG_0 per amino acid was 2.7 kcal/mol. This result is higher than previous single-molecule (0.5 to 1.5 kcal/mol) measurements, which were averaged over entire transmembrane helices (*26*, *33*). An insertion energy for a full transmembrane helix (20 to 30 amino acids) of ~12 kcal/mol is deduced from traditional ensemble measurements, yielding ~0.5 kcal/mol per amino acid (*34*). Our higher-than-anticipated result may be attributable in part to the higher energy required to solvate phenylalanines out of a lipid bilayer, to a higher ΔG_0 per amino acid when starting to unfold a helix pair relative to an average over the entire helix pair, and to the fact that the angstrom-level motion of each amino acid along the stretching axis does not lead to its full solvation in the aqueous phase; rather, it is positioned within the phospholipid interface (*35*). Future work is needed to resolve the discrepancy. However, our 1D free-energy landscape for this three–amino acid transition was robust. Specifically, we independently reconstructed a 1D free-energy landscape using an inverse-Boltzmann analysis (fig. S10C) (*36*) and measured the transition barrier position ($\Delta x^{\ddagger}$) using a Bell analysis of the average force-dependent lifetime (fig. S11) (*37*). Landscapes and landscape parameters between different methods agreed to within error, notwithstanding the well-known limitations of the Bell model (*38*) that assumes $\Delta x^{\ddagger}$ does not move as a function of applied load.

The enhanced precision achieved in these records helps to resolve a long-standing discrepancy between theoretical and experimental studies of BR unfolding, based on steered MD simulations or SMFS measurements, respectively. Specifically, prior experimental studies supplied evidence for one or two intermediate unfolding states per helix pair (~50 amino acids), whereas steered MD simulations (*23*) predicted a far denser series of unfolding intermediates, occurring once every approximately two to eight amino acids. The MD predictions, as it turns out, correspond well to the closely spaced intermediates revealed by the present work. In fact, ~60% of the unfolding intermediate states predicted with MD simulations were observed in these experiments. Expressed the other way around, ~55% of the intermediate states observed in our experiments were predicted with MD simulations (fig. S12). For helix E, in which we managed the highest resolution, a supermajority (80%) of the intermediates predicted with MD could be identified in our experimental data. Given the detail and density of unfolding intermediates, it is equally notable that SMFS detected intermediates that were otherwise absent from MD simulations, over several comparatively large regions (more than five amino acids) (fig. S12). We attribute this difference to the seven-orders-of-magnitude-greater pulling rates used in MD simulations, as compared with those of actual experiments (v = 1 m/s, versus 300 nm/s, respectively). Under the circumstances, the excellent correspondence between MD and SMFS provides increased confidence for using theoretical simulations to explore the unfolding and energetics of membrane proteins.

By using ultrashort cantilevers optimized for improved spatiotemporal resolution, we have

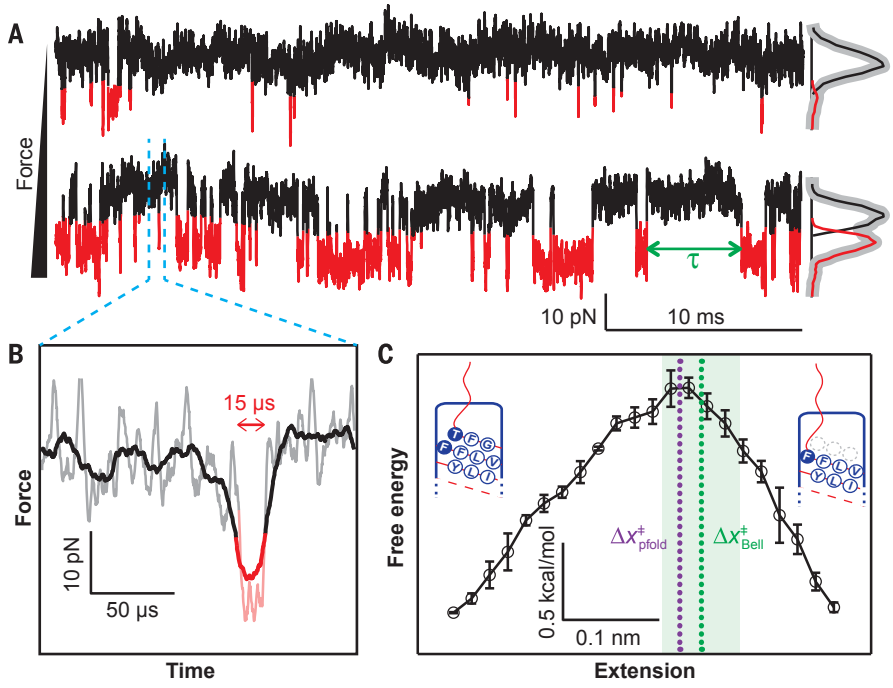

Fig. 4. Equilibrium folding of a three–amino acid segment of a membrane protein. (**A**) Force-versus-time traces show reversible transitions between two previously unresolved intermediates (I^1_{ED}, black; I^2_{ED}, red) at v = 0 nm/s. The cantilever was retracted from the surface by 0.5 nm between these two traces, increasing the force applied to the BR and shifting the equilibrium toward I^2_{ED}. Data were smoothed at 25 kHz. (**B**) A high-resolution section of the lower record in (A) illustrates detection of states that last only 15 μs. Data were smoothed at 25 kHz (black and red) and 125 kHz (gray and pink). (**C**) A reconstructed 1D free-energy landscape at $F_{1/2}$ based on the equilibrium data shown in (A) and a p_{fold} analysis (*31*). The barrier position determined by p_{fold} (purple line) agrees with the result of an independent analysis based on the Bell model (green line) (fig. S11). Error bars represent the SEM, and the light green shading represents the uncertainly in determination of $\Delta x^{\ddagger}_{Bell}$.

developed a highly detailed view of BR unfolding. Force spectroscopy has revealed a multiplicity of closely spaced, transiently occupied intermediate states, representing small changes in the molecular conformation. The widely held notion that the mechanical unfolding of BR at standard stretching rates occurred far from equilibrium is likely to be incorrect; refolding is, in fact, widespread but masked by experimental limitations when using standard cantilevers. In retrospect, elements of BR secondary structure likely unfolded and refolded during past SMFS experiments but did so faster than the force probe could respond. Last, the technique demonstrated here is by no means restricted to BR but could readily be adapted to other membrane proteins studied by using AFM (*19*) and, more generally, to studies of nucleic acid structures (*39*), mechanosensitive enzymes (*40*), and canonical globular proteins (*4*).

REFERENCES AND NOTES

1. K. A. Dill, J. L. MacCallum, *Science* **338**, 1042–1046 (2012).
2. D. M. Korzhnev, T. L. Religa, W. Banachewicz, A. R. Fersht, L. E. Kay, *Science* **329**, 1312–1316 (2010).
3. X. Zhuang *et al*., *Science* **288**, 2048–2051 (2000).
4. A. Borgia, P. M. Williams, J. Clarke, *Annu. Rev. Biochem.* **77**, 101–125 (2008).
5. P. E. Marszalek *et al*., *Nature* **402**, 100–103 (1999).
6. J. Liphardt, B. Onoa, S. B. Smith, I. Tinoco Jr., C. Bustamante, *Science* **292**, 733–737 (2001).
7. C. Cecconi, E. A. Shank, C. Bustamante, S. Marqusee, *Science* **309**, 2057–2060 (2005).
8. J. Stigler, F. Ziegler, A. Gieseke, J. C. M. Gebhardt, M. Rief, *Science* **334**, 512–516 (2011).
9. F. Oesterhelt *et al*., *Science* **288**, 143–146 (2000).
10. Y. Gao *et al*., *Science* **337**, 1340–1343 (2012).
11. B. Onoa *et al*., *Science* **299**, 1892–1895 (2003).
12. G. M. Nam, D. E. Makarov, *Protein Sci.* **25**, 123–134 (2016).
13. P. Cossio, G. Hummer, A. Szabo, *Proc. Natl. Acad. Sci. U.S.A.* **112**, 14248–14253 (2015).
14. K. C. Neuman, A. Nagy, *Nat. Methods* **5**, 491–505 (2008).
15. K. Neupane *et al*., *Science* **352**, 239–242 (2016).
16. F. Rico, L. Gonzalez, I. Casuso, M. Puig-Vidal, S. Scheuring, *Science* **342**, 741–743 (2013).
17. D. T. Edwards *et al*., *Nano Lett.* **15**, 7091–7098 (2015).
18. D. J. Müller *et al*., *Biophys. J.* **83**, 3578–3588 (2002).
19. C. A. Bippes, D. J. Muller, *Rep. Prog. Phys.* **74**, 086601 (2011).
20. K. T. Sapra, H. Besir, D. Oesterhelt, D. J. Muller, *J. Mol. Biol.* **355**, 640–650 (2006).
21. R. Petrosyan *et al*., *Nano Lett.* **15**, 3624–3633 (2015).
22. M. Zocher *et al*., *ACS Nano* **6**, 961–971 (2012).
23. C. Kappel, H. Grubmüller, *Biophys. J.* **100**, 1109–1119 (2011).
24. M. Jahn, J. Buchner, T. Hugel, M. Rief, *Proc. Natl. Acad. Sci. U.S.A.* **113**, 1232–1237 (2016).
25. H. S. Chung, K. McHale, J. M. Louis, W. A. Eaton, *Science* **335**, 981–984 (2012).
26. M. Kessler, K. E. Gottschalk, H. Janovjak, D. J. Muller, H. E. Gaub, *J. Mol. Biol.* **357**, 644–654 (2006).
27. J. P. Junker, F. Ziegler, M. Rief, *Science* **323**, 633–637 (2009).
28. C. He *et al*., *Angew. Chem. Int. Ed. Engl.* **54**, 9921–9925 (2015).
29. M. T. Woodside, S. M. Block, *Annu. Rev. Biophys.* **43**, 19–39 (2014).
30. Y. Zhang, O. K. Dudko, *Proc. Natl. Acad. Sci. U.S.A.* **110**, 16432–16437 (2013).
31. Y. M. Rhee, V. S. Pande, *J. Phys. Chem. B* **109**, 6780–6786 (2005).
32. A. P. Manuel, J. Lambert, M. T. Woodside, *Proc. Natl. Acad. Sci. U.S.A.* **112**, 7183–7188 (2015).
33. J. Preiner *et al*., *Biophys. J.* **93**, 930–937 (2007).
34. F. Cymer, G. von Heijne, S. H. White, *J. Mol. Biol.* **427**, 999–1022 (2015).
35. G. von Heijne, *Nat. Rev. Mol. Cell Biol.* **7**, 909–918 (2006).
36. M. T. Woodside *et al*., *Science* **314**, 1001–1004 (2006).
37. G. I. Bell, *Science* **200**, 618–627 (1978).
38. O. K. Dudko, G. Hummer, A. Szabo, *Phys. Rev. Lett.* **96**, 108101 (2006).
39. A. Savinov, C. F. Perez, S. M. Block, *Biochim. Biophys. Acta* **1839**, 1030–1045 (2014).
40. E. M. Puchner, H. E. Gaub, *Annu. Rev. Biophys.* **41**, 497–518 (2012).

ACKNOWLEDGMENTS

We thank L. Randall for providing halobacterium and protocols for preparing BR samples, L. Uyetake for purifying BR, G. King and A. Churnside for initial AFM studies of BR, M. Woodside for critical reading of the manuscript, and G. Emmanuel for sharing code for a hidden Markov model. The data presented in this paper, including supplementary figures, is available via Dryad (http://dx.doi.org/10.5061/dryad.g0n2d). This work was supported by a National Institute of Health Molecular Biophysics Training Grant Slot to M.G.W.S. (T32 GM-065103), a National Research Council Fellowship to D.T.E., the National Science Foundation (DBI-135398; Phys-1125844), and National Institute of Standards and Technology (NIST). T.T.P. is a staff member of NIST's quantum physics division.

SUPPLEMENTARY MATERIALS

www.sciencemag.org/content/355/6328/945/suppl/DC1
Materials and Methods
Figs. S1 to S13
Table S1
References (*41*–*47*)

3 August 2016; accepted 6 February 2017
10.1126/science.aah7124

Hidden dynamics in the unfolding of individual bacteriorhodopsin proteins

Hao Yu, Matthew G. W. Siewny, Devin T. Edwards, Aric W. Sanders and Thomas T. Perkins

Science **355** (6328), 945-950.
DOI: 10.1126/science.aah7124

Pulling apart protein unfolding

Elucidating the details of how complex proteins fold is a longstanding challenge. Key insights into the unfolding pathways of diverse proteins have come from single-molecule force spectroscopy (SMFS) experiments in which proteins are literally pulled apart. Yu *et al.* developed a SMFS technique that could unfold individual bacteriorhodopsin molecules in a native lipid bilayer with 1-μs temporal resolution (see the Perspective by Müller and Gaub). The technique delivered a 100-fold improvement over earlier studies of bacteriorhodopsin and revealed many intermediates not seen before. The authors also observed unfolding and refolding transitions between intermediate states.

Science, this issue p. 945; see also p. 907